Polymer Chemistry

PAPER

Check for updates

Ethylene polymerization using heterogeneous multinuclear nickel catalysts supported by a crosslinked alpha diimine ligand network†

Keaton M. Turney, [ID] Parin Kaewdeewong and James M. Eagan [ID] *

Nickel(II) alpha diimine catalysts typically produce high molecular weight low crystallinity amorphous polyethylenes *via* a chain-walking propagation mechanism consisting of consecutive beta hydrogen elimination and reinsertion reactions. In this report the synthesis of a crosslinked alpha diimine ligand and metalation with $NiBr_2(dme)$ affords a multinuclear heterogeneous pre-catalyst which exhibits significant differences from the homogeneous analogue: reduced chain-walking, slower termination, and higher activities. Whereas the homogeneous analogues are known to afford polyethylenes with low crystallinity, high molecular weights, and high activity (<1% crystallinity, 163 kDa, and 520 kg PE mol Ni^{-1} h^{-1}, respectively), the heterogeneous system under identical conditions yielded polyethylene with increases in all three parameters (20% crystallinity, 217 kDa, and 1377 kg PE mol Ni^{-1} h^{-1}, respectively). The branching content was further characterized by quantitative ^{13}C NMR to reveal that not only did the alkyl branches decrease in number, but also in average branch length, indicative of a decreased propensity for the multinuclear catalyst to chain-walk. Several advantages of heterogeneous catalysis were also observed including the removal of hazardous metal residue, gas-phase polymerization, co-catalyst recovery, and less reactor fouling.

Introduction

Ziegler–Natta olefin polymerization is among the most energy efficient methods for producing durable and mechanically recyclable synthetic materials.[1] The advent of late-transition metal olefin polymerization catalysts[2–4] has provided synthetic methodologies capable of tuning the branching,[5–8] block structure,[9–12] topology[13] and functionality of polyolefins.[14–16] In Brookhart's seminal report, ethylene was polymerized with diisopropyl aniline derived α-diimine $NiBr_2$ pre-catalysts (**1**, Fig. 1) and methyl aluminoxane (MAO) co-catalyst to produce branched linear low-density polyethylenes (PE) physically comparable to ethylene-*co*-propylene (EP) rubber.[3] When sourced from appropriate crops, bio-ethylene has the potential to be both carbon-negative and commercially viable.[17] Consequently, it is important to advance the tailored design of sustainable ethylene-based materials through catalysis and polymer chemistry.

Multinuclear polymerization catalysts (**2**) often exhibit unique selectivities, increased comonomer incorporation, and enhanced activities because of intramolecular metal–metal cooperative effects.[18–25] These cooperative effects depend on the ligand linker as well as the nature of the metals. In regards to Ni(II) α-diimine multinuclear catalysts, Soares and coworkers found a rigid aryl link dinuclear catalyst (**2**; R_1 = acenaphthene) exhibited the highest activity (3280 kg PE mol Ni^{-1} h^{-1}) relative to other linkers or the homogeneous analogue (**1**; 2220 kg PE mol Ni^{-1} h^{-1}) when activated with methyl aluminoxane (MAO) co-catalyst under their conditions.[26] The dinuclear cooperative effects impacted the branching density (N_b) and distribution by decreasing the overall N_b (75 to 40 CH_3/1000 C) and increasing the formation of hexyl branches (from 2 to 20 mol%). Similar findings were made by Redshaw and coworkers with methylene linked dinuclear catalysts in regards to increased activities (5430 to 7860 kg PE mol Ni^{-1} h^{-1}) and higher molecular weights relative to mononuclear analogues (102 000 to 205 000 g mol^{-1}).[27] Redshaw further explored the *ortho* substitution of the aniline diimine which is known to profoundly impact activity, molecular weights, and branching.[5] Chen and coworkers designed dinuclear acenaphthene α-diimine catalysts with a conjugated backbone, which produced amorphous PE with nearly twice the activity (474 kg PE mol Ni^{-1} h^{-1}) of the mononuclear catalyst (**1**: 260 kg PE mol Ni^{-1} h^{-1}) and with higher branching density (80 to 111 CH_3/1000 C) due to the electron deficient Ni center and ligand conjugation when activated with modified methyl aluminoxane

School of Polymer Science and Polymer Engineering, The University of Akron, Akron, Ohio, 44325-3909 USA. E-mail: eagan@uakron.edu
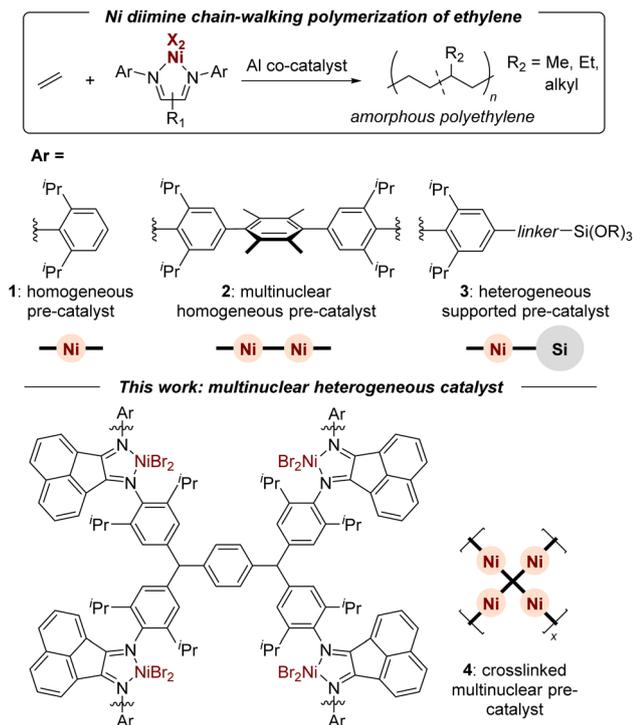
Fig. 1 Chain-walking ethylene polymerization catalyzed by homogeneous, multinuclear, and heterogeneous Ni α-diimine pre-catalysts.

(MMAO) cocatalyst under their conditions.[28] Chen's dinuclear catalyst also exhibited higher molecular weights than the mononuclear analogue (166 000 to 183 000 g mol^{-1}). Dinuclear and multinuclear dendritic Ni(II) iminopyridine catalysts have been studied in the oligomerization of ethylene, but do not yield high molecular weight polymers due to the lack of steric blocking of the axial site of the active metal center.[29–32]

A second strategy for enhanced control and efficiency in late-transition metal olefin polymerization is heterogenization of the active sites (**3**, Fig. 1).[33–51] The heterogenization of late-transition metal catalysts improves their recyclability,[33–36] enables gas-phase solvent-free conditions,[37–42] and facilitates the removal of metal residues from the final product.[33,35] The latter point is particularly important for industrial applications of Ni catalysts due to health hazards.[43] Methods for heterogenization can be organized into physisorption and covalent linking of metal pre-catalyst or Al co-catalyst to a support (*e.g.*, silica).[44] For example, Brookhart demonstrated silane linkers covalently tethered to the aryl α-diimine ligand yield silica supported heterogeneous catalysts with higher activities (10-fold) relative to silica-bound MAO derived catalysts.[37] In the work of de Souza and coworkers, a Ni(II) α-diimine catalyst was supported on silica-bound MAO to form a heterogeneous catalyst yielding higher molecular weight PE with fewer branches (30 to 14 CH$_3$/1000 C) in combination with a homogeneous Ni(II) α-diimine catalyst.[49] Conley and coworkers utilized the ionic physisorption of sulfonated ligands onto inorganic zirconia as a heterogenization strategy without significantly altering the

polymerization properties relative to the homogeneous analogue.[45] Recently a number of novel strategies have emerged for heterogenization of other late-transition metal catalysts, including hydrogen bonding,[46] self-assembled ionic clusters,[47] and micelle encapsulation.[48] While most heterogeneous systems help to prevent reactor fouling and simplify catalyst removal, they suffer from decreased activities and require higher loadings of aluminum co-catalyst.[46,49–51]

This work reports a complementary strategy for the heterogenization of Brookhart α-diimine catalysts in which a crosslinked ligand supports multiple active sites with chain-walking behavior. The resulting system (**4**) exhibits desirable heterogeneous properties such as catalyst removal. The high concentration of active sites, relative to other supported catalysts, allows for lower aluminum co-catalyst loadings and enhances polymerization activities through multinuclear cooperative effects. Through catalyst and reaction design, a single sustainably sourced monomer feedstock was converted into durable materials with a range of thermal properties.

Results and discussion

Our approach to synthesizing crosslinked α-diimine ligand networks (Scheme 1) revolves around the design and synthesis of the tetra-aniline molecule **7**—the Friedel–Craft alkylation product of 2,6-diisopropyl aniline (**5**) and terephthaldehyde (**6**). Combining these reagents in refluxing 2 M HCl and 300 mol% (to **6**) ZnCl$_2$ affords tetra-aniline **7** in 45% yield after crystallization from CH$_2$Cl$_2$/MeOH as a pale violet powder.[52,53] Refluxing the tetra-aniline product with acenapthenequinone (1 : 1 molar ratio of amine : carbonyl) in PhMe with 13 mol% *p*-toluenesulfonic acid for 48 h results in a dark red precipitate which was washed with PhMe and CH$_2$Cl$_2$ sequentially (46% yield). The red precipitate was ground with a mortar and pestle until fine particles were obtained. Metalation using NiBr$_2$(dimethoxyethane) was carried out by first dissolving the metal precursor in anhydrous THF for 24 h, which results in the formation of a violet solution, then addition of the insoluble crosslinked ligand and stirring for 48 h. The intensity
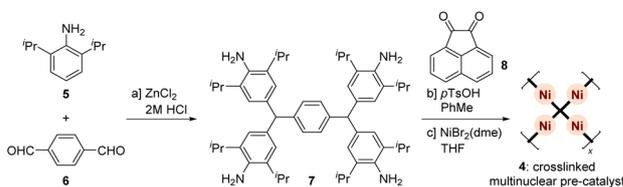
Scheme 1 The synthesis of tetra-aniline **7**, crosslinked α-diimine ligand, and metalation to pre-catalyst **4**. Reagents and conditions: [a] 2,6-diisopropylaniline (80 mmol, 4 equiv.), terephthaldehyde (20 mmol, 1 equiv.), ZnCl$_2$ (60 mmol, 3 equiv.), HCl (400 mL, 2 M), reflux, 24 h; 45% yield of **7**. [b] Acenaphthenequinone (2 mmol, 2 equiv.), tetraaniline **7** (1 mmol, 1 equiv.), pTsOH (0.125 mmol, 0.125 equiv.), PhMe (100 mL), reflux, 48 h. [c] NiBr$_2$(dme) (0.2 mmol, 2 equiv. relative to diimine functionality), crosslinked ligand from (b) (0.10 mmol diamine functionality), THF (15 mL), 25 °C, 48 h, 46% yield of **4**.

of the violet solution decreases throughout the duration of the experiment, ending with a faint violet solution indicating complexation of the $NiBr_2$ adduct by the diimine framework. The complex was filtered, rinsed with THF and pentane, after which the solids were dried under vacuum. In order to determine the degree of the metalation, the Ni content of the precatalyst was analyzed by inductively coupled plasma-optical emission spectrometry (ICP-OES) which revealed 83% of theoretical α-diimine moieties were metalated (Fig. S35 and Table S2†).

The chemical composition of the network was further characterized using Fourier-transform infrared spectroscopy (FT-IR). During the crosslinking condensation reaction, disappearance of both the acenaphthenequinone 1,2-dicarbonyl ($1719\ cm^{-1}$) and the tetra-aniline NH_2 ($3382\ \&\ 3486\ cm^{-1}$) moieties was observed (Fig. S33†). These disappearing signals are accompanied by the appearance of a signal at $1634\ cm^{-1}$ characteristic of imine stretches, suggesting successful ligand formation. However, despite full conversion of the starting materials we detected small resonances at $1737\ cm^{-1}$, which are consistent with keto-imine mono condensation products.[27] This moiety impacts the resulting degree of metalation. By comparing the ligand molecular weight and Ni content by ICP-OES we determined that 83% of the catalyst is the Ni(ɪɪ) alpha diimine structure (**4**), with the remainder as these unmetallated network defects.

Surface area and topographical features were observed by scanning electron microscopy (SEM) in both the ligand and metalated pre-catalyst (Fig. 2). After metalation with $NiBr_2(dme)$ in THF, morphological changes were evident (Fig. 2a and b; additional SEM provided in Fig. S42 and S43†). The Ni(ɪɪ) pre-catalyst is a high surface area non-porous heterogeneous solid. The long-range crystalline order was probed by X-ray powder diffraction (PXRD) which revealed a set of 9.6° and 17.9° diffraction peaks. Although the signals can be distinguished, they are dominated by the amorphous halo ranging from 5° to 50° (Fig. 2c). Considering our observation of irregular pores by high-resolution SEM along with the low degree of crystallinity observed by PXRD, it is concluded under these conditions that no ordered covalent organic frameworks are present.[54]

The polymerization of ethylene was studied for both the heterogeneous multinuclear pre-catalyst **4** and the homogeneous analogue **1**. When **1** was activated with 100 equivalents of $^i Bu_2 AlCl$ co-catalyst under 3 atm of ethylene for 60 minutes (Table 1, entry 1), amorphous ($N_b = 85\ CH_3/1000$ C) PE rubber ($M_n = 163\,000\ g\ mol^{-1}$) was obtained with high activity (520 kg PE mol $Ni^{-1}\ h^{-1}$). Interestingly, despite the same *ortho* substituents on the aniline, the heterogeneous multinuclear catalyst $4/^i Bu_2 AlCl$ yielded a PE with higher molecular weights ($M_n = 217\,000\ g\ mol^{-1}$), higher activity (1377 kg PE mol $Ni^{-1}\ h^{-1}$), and a significant increase in crystallinity ($\chi_c = 20.0\%$; $T_m = 118\ °C$; $N_b = 43$) under identical conditions (Table 1, entry 5).

We attribute the increased molecular weight, increased activity, and reduced chain-walking behavior to the cooperative effects between the Ni centers—since the *ortho*-aryl groups are consistent between the homogeneous and heterogeneous ligands. The nature of these cooperative effects is multifold and includes increased monomer concentration, proximal electrostatics, and secondary agostic interactions.[55–58] The close proximity of multiple Ni sites leads to an increase in the local ethylene concentration *via* the alkyl-ethylene Ni complex resting state.[3] Additionally, the proximity of cationic species enhances the electrophilicity of the coordinately unsaturated Ni centers for olefin enchainment.[57] Accordingly, the rate of migratory insertion relative to chain-walking and chain-transfer reactions yields a more linear and a higher molecular weight PE. It has also been proposed that secondary, possibly agostic, interactions between proximate metal centers may bias chain conformations.[57] In the case of Ni-catalyzed chain-walking polymerization, these conformational states influence the degree of branching and the branch identity.[7]

One unique property we observed in catalyst $4/^i Bu_2 AlCl$, was a strong dependence of the chain-walking behavior on reaction temperature (Table 1, entries 5–7). At 25 °C, the catalyst yields the aforementioned semi-crystalline polymers (Table 1, entry 5) with a T_m of 118 °C and $\chi_c = 20\%$. Decreasing the temperature of the reaction to 0 °C yields a polymer with a higher T_m of 128 °C and drastically increased $\chi_c = 50\%$ (Table 1, entry 6). Increasing the temperature to 80 °C results in an unobservable T_m ($\chi_c < 1\%$) and T_g of −57 °C, by DSC (Table 1, entry 7). There are relatively few Ni(ɪɪ) α-diimine catalysts we are aware of that have shown the ability to produce this range of high T_m plastics or amorphous rubbers under mild pressures and temperatures (0–80 °C).[10–12]
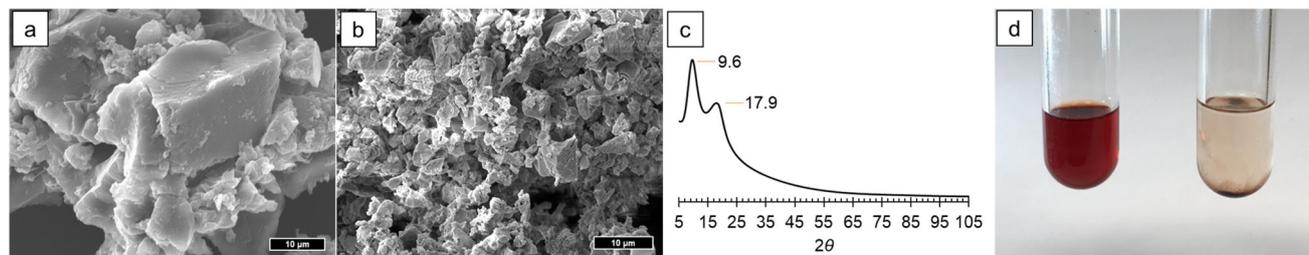

Fig. 2 (a) SEM image of the ligand. (b) SEM image of pre-catalyst **4**. (c) PXRD spectra of the ligand. (d) Image of pre-catalysts **1** (left) and **4** (right) in PhMe.

Table 1 Polymerizations conducted in PhMe (100 mL) with 10 μmol of pre-catalyst **4** (pre-catalyst **1** used for entries 1 and 2) activated with ^{i}Bu$_2$AlCl (1 mmol, 100 equiv.).

Entry (#)	C$_2$H$_4$ (atm)	T_{rxn} (°C)	t_{rxn} (min)	Yield (g)	Activity[a] (kg PE mol Ni^{-1} h^{-1})	M_n[b] (kg mol^{-1})	$Đ$ (M_w/M_n)[b]	N_b (CH$_3$/1000 C)[c]	T_m[d] (°C)	ΔH_f[d] (J g^{-1})	X[e] (%)
1 (cat. **1**)	3	25	60	5.2	520	163	2.27	85	N.D.	N.D.	<1.0
2 (cat. **1**)	3	80	60	5.6	565	67	2.56	104	N.D.	N.D.	<1.0
3	1	25	60	3.1	301	262	3.19	45	114	55	15.7
4	5	25	60	14.1	1391	266	3.75	32	120	83	28.3
5	3	25	60	13.8	1377	217	3.52	43	118	58	20.0
6	3	0	60	0.7	70	409	4.05	7	128	146	50.0
7	3	80	60	3.4	332	68	3.33	97	N.D.	N.D.	<1.0
8	3	25	30	9.0	1805	149	3.88	44	113	52	17.8
9	3	25	10	1.9	1429	134	4.02	37	114	65	21.9
10[f]	3	25	60	3.8	343	79	5.02	65	112	27	9.1

[a] Activity = kg PE mol per Ni per hour. [b] Determined by gel-permeation chromatography using 1,2,4-trichlorobenzene at 140 °C relative to polystyrene standards. [c] Alkyl branches (CH$_3$) per 1000 carbons (N_b) determined from ^{1}H NMR using 1,1,2,2-tetrachloroethane as solvent at 125 °C.[59] [d] Determined from differential scanning calorimetry of the second heating cycle with a heating rate of 10 °C min^{-1}. [e] Calculated using the enthalpy of fusion for crystalline PE (ΔH_f = 293 J g^{-1}).[60] [f] Gas-phase polymerization.

The chain-walking mechanism was further investigated by analyzing the polymer microstructures. Fig. 3 shows the N_b determined by ^{1}H NMR and the branch identity distribution from ^{13}C NMR.[59,61] Of interest, the PE rubber from the crosslinked catalyst **4**/^{i}Bu$_2$AlCl (Table 1, entry 7) contains shorter branches than the homogeneous analogue **1**/^{i}Bu$_2$AlCl (Table 1, entry 2). At 80 °C, the homogeneous and heterogeneous catalysts yielded PEs with similar branching numbers (N_b = 104 and 97, respectively). Higher molecular weights and dispersities were also observed in PE produced from catalyst **4**/^{i}Bu$_2$AlCl. Under identical conditions, catalyst **1**/^{i}Bu$_2$AlCl

yields a polymer with M_n = 163 kDa and $Đ$ = 2.27 (Table 1, entry 1), whereas catalyst **4** produces PE with M_n = 217 kDa and $Đ$ = 3.52 (Table 1, entry 5). The higher molecular weights observed with catalyst **4**/^{i}Bu$_2$AlCl is attributed to cooperative effects as previously described. The broadening of dispersity is attributed to the heterogeneous nature of the catalyst.

Activity was also investigated at different times of polymerization (Table 1, entries 5, 8 and 9). The 30-minute polymerization had the highest activity (1805 kg PE mol Ni^{-1} h^{-1}), followed by the 10-minute polymerization (1429 kg PE mol Ni^{-1} h^{-1}), and finally the 60-minute reaction (1377 kg PE mol Ni^{-1} h^{-1}). Since alkyl aluminum activation of nickel dibromide catalysts is relatively fast (<100 s)[26] we expect these differences result from a combination of reaction exotherms, catalyst deactivation, as well as the initiation kinetics.

To determine the efficacy of various co-catalysts in activating **4** (Table 2 and Fig. 4), two alkylaluminum chlorides were chosen, ^{i}Bu$_2$AlCl and Et$_2$AlCl, as well as two aluminoxanes, modified-methyl aluminoxane (MMAO) and methyl aluminoxane-improved performance (PMAO-IP). Interestingly, while PMAO-IP and MMAO co-catalysts yielded higher crystallinity, the yields were dramatically decreased relative to the small molecule alkylaluminum chloride co-catalysts. We attribute this observation to the sterically hindered environment of the crosslinked catalyst's Ni centers and the oligomeric structure of MAO activators.[62–65]

The decreased yield observed in polymerizations using MMAO and PMAO-IP suggests that these aluminoxane com-
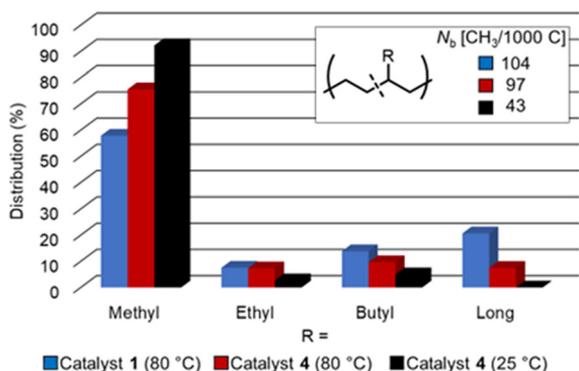
Fig. 3 Branching numbers and distributions of PE samples acquired by ^{1}H NMR and ^{13}C NMR, respectively.

Table 2 Polymerizations were conducted in PhMe (100 mL) with 10 μmol of pre-catalyst **4** (pre-catalyst **1** used for entry 1) activated with aluminum co-catalyst (1 mmol, 100 equiv.) for 60 minutes

Entry (#)	Co-catalyst	C_2H_4 (atm)	T_{rxn} (°C)	Yield (g)	Activity[a] (kg PE mol Ni^{-1} h^{-1})	M_n[b] (kg mol^{-1})	$Đ$ (M_w/M_n)[c]	N_b (CH_3/1000 C)[c]	T_m[d] (°C)	ΔH_f[d] (J g^{-1})	X[e] (%)
1 (cat. **1**)	$^iBu_2AlCl$	3	25	5.2	520	163	2.27	85	N.D.	N.D.	<1.0
2	PMAO-IP	3	25	0.5	46	301	4.92	10	127	121	41.1
3	MMAO	3	25	0.5	52	283	5.37	17	126	116	39.6
4	Et_2AlCl	3	25	7.9	763	258	4.42	25	120	100	34.3
5	$^iBu_2AlCl$	3	25	13.8	1377	217	3.52	43	118	58	20.0
6	$^iBu_2AlCl$	5	0	1.0	102	409	4.05	4	130	129	44.1
7	PMAO-IP	5	0	0.33	33	321	4.33	4	130	132	45.1

[a] Activity = kg PE mol per Ni per hour. [b] Determined by gel-permeation chromatography using 1,2,4-trichlorobenzene at 140 °C relative to polystyrene standards. [c] Alkyl branches (CH_3) per 1000 carbons (N_b) determined from ^1H NMR using 1,1,2,2-tetrachloroethane as solvent at 125 °C.[59] [d] Determined from differential scanning calorimetry of the second heating cycle with a heating rate of 10 °C min^{-1}. [e] Calculated using the enthalpy of fusion for crystalline PE ($\Delta H_f = 293$ J g^{-1}).[60]
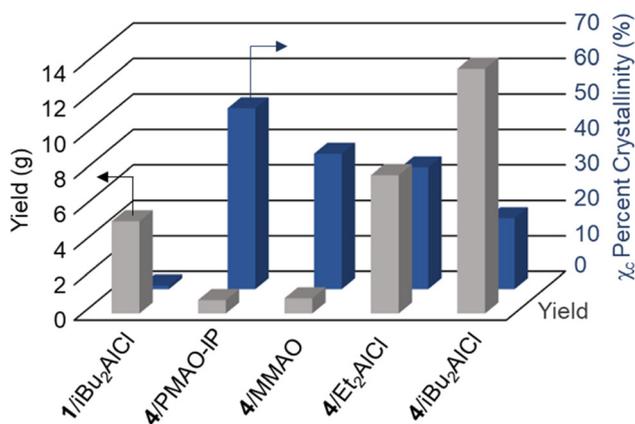
Fig. 4 Effects of co-catalyst on yield and crystallinity of PE samples produced by pre-catalysts **1** and **4**. Reagents and conditions: PhMe (100 mL), Ni catalyst (10 μmol), Al activator (1 mmol, 100 equiv.), ethylene (3 atm), 25 °C, 1 h.

pounds are not effectively activating all of the Ni sites of the catalyst due to the larger oligomeric aluminoxanes and the steric environment of the heterogeneous catalyst. Additionally, the MMAO and PMAO-IP induce different catalytic behavior than alkylaluminum chloride activators because of the resulting ion-pair with Ni. Previous reports have shown Ni/MMAO catalysts exhibit higher chain-propagation rates because of sterics and loose ion pairing.[65–68] In our study, the increased propagation rate of **4**/aluminoxanes, albeit fewer active sites, yields higher crystallinity PE.[4,65]

It has been reported that a more electron deficient Ni center leads to increased branching density and decreased molecular weight of the polymer.[69] Activation by alkylaluminum chlorides increases the Lewis acidity of the active Ni sites,[64] and affords polymerizations with higher rates of chain-walking (Table 2, entries 4 and 5). Combining this knowledge, the high crystallinity PEs ($T_m = 130$ °C, and $\chi_c = 44.1\%$ and 45.1%) were synthesized from pre-catalyst **4** at 5 atm of ethylene and 0 °C, with either $^iBu_2AlCl$ (Table 2, entry 6) or PMAO-IP (Table 2, entry 7), respectively.

A gas phase reaction was demonstrated by suspending the pre-catalyst in 2 mL of PhMe, introducing 100 equiv. of $^iBu_2AlCl$ co-catalyst and then removing the excess Al-solution (Table 1, entry 10). Upon injection of ethylene, an exotherm was qualitatively observed along with PE propagation. At the end of the reaction, the polymer was removed from the reactor with minimal to no residue adhering to the glass vessel. Polymers from slurry-phase and gas-phase polymerizations were optically characterized *via* SEM (Fig. 5a and b). The polymer could then be separated from residual Ni using Soxhlet extraction with refluxing toluene to afford a colorless product (Fig. 5c). The extraction efficacy was quantified using ICP-OES which revealed 97% of the Ni were removed from the precipitated polymer (0.32 ppm Ni) by the extraction process (0.01 ppm Ni).

Experimental

General slurry-phase polymerization of ethylene

A glass pressure vessel (6 oz) and stir bar were dried overnight in an oven at 150 °C. To this vessel, in a nitrogen filled glovebox was added pre-catalyst in PhMe (2 mL), and co-catalyst in PhMe (2 mL), followed by the remaining PhMe (100 mL total volume). The pressure head assembly was fixed to the vessel, removed from the glovebox, and equilibrated at the reaction
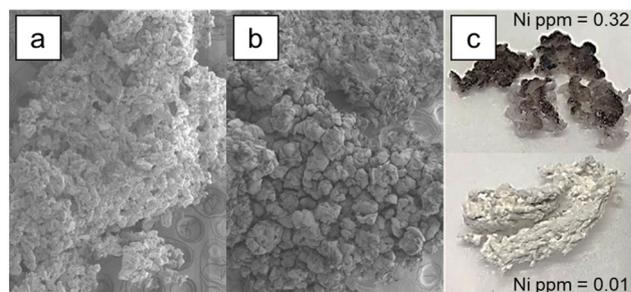
Fig. 5 (a) SEM image of PE from Table 1, entry 5 (slurry-phase). (b) SEM image of PE from Table 1, entry 10 (gas-phase). (c) Precipitated gas-phase PE (top) and Soxhlet-extracted gas-phase PE (bottom).

temperature before introducing ethylene. The pressure of ethylene, reaction temperature, and time was varied according to Table 1. At the end of the experiment, the ethylene supply was closed and the reactor was vented, and 5 mL of 5% (v/v) HCl in MeOH was injected and stirred for an additional 5 minutes. The reactor was then disassembled and the polymer was precipitated in 250 mL of MeOH, isolated *via* vacuum filtration, and dried in a vacuum oven at 60 °C overnight in preparation for characterization.

Gas-phase polymerization of ethylene

A glass pressure vessel (6 oz) and stir bar were dried overnight in an oven at 150 °C. To this vessel, in a nitrogen filled glovebox was added pre-catalyst, PhMe (2 mL), and co-catalyst. The suspended catalyst was allowed to settle to the bottom of the reactor and the excess co-catalyst solution was removed by pipette. The pressure head assembly was fixed to the vessel, removed from the glovebox, and 3 atm of ethylene was introduced into the system. A qualitative exotherm was observed and ethylene pressure was maintained for 60 minutes, during which time PE particle growth was observed. After the 1 hour reaction time, the ethylene supply was closed, the reactor vented, and 5 mL of 5% (v/v) HCl in MeOH was injected and stirred for an additional 5 minutes. The reactor was disassembled and the polymer was removed from the vessel using a plastic spatula with little to no observable PE residue left lining the vessel walls. The PE sample was dried in a vacuum oven at 60 °C overnight in preparation for characterization.

Synthesis of tetra-aniline (7); (4,4′,4″,4‴-(1,4-phenylenebis(methanetriyl))tetrakis(2,6-diisopropylaniline))

In a 1 L round-bottom flask, 2,6-diisopropyl aniline (14.20 g, 80 mmol) was added to 2 M HCl (400 mL) to yield a white precipitate. To the slurry was added terephthaldehyde (2.68 g, 20 mmol) followed by solid $ZnCl_2$ (8.16 g, 60 mmol). The mixture was then heated to reflux for 20 hours, during which time the reaction turned blue in color. The reaction was cooled to room temperature and 6 M NaOH was added dropwise, carefully to avoid excessive exothermic reaction, until pH = 10. The precipitate that formed was filtered, collected, and recrystallized in hot methanol/dichloromethane. The isolated solids from $MeOH/CH_2Cl_2$ recrystallization were subsequently dissolved in CH_2Cl_2 (200 mL), filtered, and the CH_2Cl_2 soluble fraction was evaporated to dryness to afford the violet tetra-aniline (7) (7.30 g, 45% yield). ^1H NMR (500 MHz, $CDCl_3$): δ 6.99 (s, 1H), 6.80 (s, 1H), δ 5.27 (s, 1H), 3.50 (s, 1H), 2.93–2.84 (m, J = 6.7 Hz, 1H), 1.17–1.15 (d, J = 6.7 Hz, 6H). ^{13}C NMR (500 MHz): δ 143.23, 137.71, 135.00, 132.26, 128.92, 123.97, 56.26, 28.03, 22.63. HRMS (ESI-MS): exact mass [M] calculated for $C_{56}H_{78}N_4$, 806.6208. $[M + H]^+$ detected at 807.6240. FT-IR (ATR): primary amine (N–H) stretching (3486, 3382 cm^{-1}), primary amine (N–H) deformation (1621 cm^{-1}).

Synthesis of crosslinked ligand

Tetra-aniline (7) (1.00 mmol, 0.807 g), acenaphthenequinone (2.00 mmol, 0.365 g), and *p*-toluenesulfonic acid (0.125 mmol,

0.025 g) were added to a 500 mL round–bottom flask. To the flask was added 100 mL of PhMe. The mixture was stirred vigorously and refluxed for 48 hours with a Dean–Stark adapter. The insoluble dark red solids that formed became suspended in the PhMe and lined the flask walls during the course of the reaction. The flask was removed from heat and the mixture was filtered *via* vacuum filtration. The solids were rinsed three times with CH_2Cl_2 (20 mL). The solids were transferred to a mortar and pestle and ground from flakey small particles (*ca.* 1–2 mm), vacuum filtered, and transferred back to the mortar and pestle for further grinding in order to acquire a fine powder (*ca.* <0.5 mm particles). This final powder was vacuum filtered and rinsed with three washes of CH_2Cl_2 (20 mL). The crosslinked ligand was collected as dark red powder and transferred to a vial to be dried in a vacuum oven overnight at 60 °C (0.455 g, 46% yield). FT-IR (ATR): imine (N=C) stretching (1627 cm^{-1}) observed. No primary amine (N–H) stretching observed (1650–1590 cm^{-1}). No α-diketone (C=O) stretching observed (1730–1710 cm^{-1}).

Metalation of crosslinked catalyst (4)

In a nitrogen filled glovebox, nickel(ɪɪ) bromide (dimethoxyethane adduct) (0.20 mmol, 0.617 g) was added to a 20 mL vial and dissolved in 15 mL of anhydrous THF, during which a violet solution immediately formed. The solution was stirred for 24 hours for complete solvation. To this vial, the crosslinked ligand (0.10 mmol, 0.055 g) was added and stirred for an additional 48 hours. Over the duration of the experiment, the intensity of the violet color decreased as it transitioned to a faint red solution. Once complete, the reaction stirring was stopped and the catalyst was allowed to settle to the bottom of the vial. The supernatant solution was removed carefully using a pipette. The remaining catalyst was washed once with THF (3 mL), followed by three washes with pentane (3 mL). The crosslinked catalyst (4) was obtained as a dark red powder (0.059 g, 77% yield).

Extraction of catalyst from polymer

For heterogeneous catalyst removal, crude polymer with a red/brown color was loaded into a 33 × 118 mm cellulose Soxhlet thimble. A Soxhlet extraction was performed for 24 hours using PhMe (200 mL). After 24 hours, the apparatus was cooled to yield a translucent solution. The PhMe was concentrated to approximately 50 mL at which point the polymer was precipitated in MeOH (250 mL). Colorless polymer was observed and recovered *via* vacuum filtration. The polymer was dried *via* vacuum oven for a quantitative yield.

ICP-OES sample preparation

A Ni standard solution was acquired (10 ppm) and standards of 0, 2.5, 5, 7.5, and 10 ppm were prepared *via* serial dilution in volumetric flasks (10 mL). Catalyst samples were massed in a 2-dram vial and digested for 24 hours in trace metal grade nitric acid (0.5 mL). After 24 hours, the red/brown catalyst had digested into a yellow solution. This solution was diluted with ultra-pure H_2O in a volumetric flask (10 mL). Polymer samples

were first degraded by combustion in a borosilicate test-tube over an open flame to improve digestion efficiency. The samples were then digested in trace metal grade nitric acid (1 mL) for 96 hours after which a pale-yellow solution was extracted and diluted with ultra-pure pure H_2O in a volumetric flask (25 mL). Prior to data acquisition, the Ni standards were analyzed to create a standard curve by analysis at a wavelength of 234.601 nm and required to achieve a linear fit of $R^2 >$ 0.995.

Conclusions

This work demonstrates a complementary strategy to controlling polyethylene microstructure from cationic α-diimine Ni(II) pre-catalysts. The multinuclear crosslinked system **4**/^{i}Bu$_2$AlCl exhibits high activities, recovery of excess co-catalyst, and gas phase reactivity while producing polyethylenes with high melting temperatures, short branch lengths, and low concentrations of residual Ni. When compared to homogeneous counterparts these reactivity differences are derived from multinuclear cooperativity effects rather than the *ortho*-substituents of the aniline or backbone moieties which are more prevalent in prior work. Additionally, a broad range of polyethylene branching and thus plastic or rubbery thermal behavior can be accessed within a narrow window of mild polymerization temperatures and pressures. The described heterogeneous catalyst design serves to expand the utility of ethylene as a single feedstock for tailored polyethylene microstructures and minimal catalyst residue.

Author contributions

JE and KMT conceptualized; KMT and PK acquired, analyzed, and validated data; all authors contributed to manuscript writing, reviewing, and editing.

Conflicts of interest

There are no conflicts to declare.

Acknowledgements

References

1 M. Stürzel, S. Mihan and R. Mülhaupt, *Chem. Rev.*, 2016, **116**, 1398–1433.

2 F. Wang and C. Chen, *Polym. Chem.*, 2019, **10**, 2354–2369.

3 L. K. Johnson, C. M. Killian and M. Brookhart, *J. Am. Chem. Soc.*, 1995, **117**, 6414–6415.

4 S. D. Ittel, L. K. Johnson and M. Brookhart, *Chem. Rev.*, 2000, **100**, 1169–1203.

5 D. P. Gates, S. A. Svejda, E. Onate, C. M. Killian, L. K. Johnson, P. S. White and M. Brookhart, *Macromolecules*, 2000, **33**, 2320–2334.

6 T. Vaidya, K. Klimovica, A. M. Lapointe, I. Keresztes, E. B. Lobkovsky, O. Daugulis and G. W. Coates, *J. Am. Chem. Soc.*, 2014, **136**, 7213–7216.

7 Y. Zhang, X. Kang and Z. Jian, *Nat. Commun.*, 2022, **13**, 725.

8 A. M. Doerr, M. R. Curry, R. C. Chapleski, J. M. Burroughs, E. K. Lander, S. Roy and B. K. Long, *ACS Catal.*, 2022, **12**, 73–81.

9 K. S. O'Connor, A. Watts, T. Vaidya, A. M. LaPointe, M. A. Hillmyer and G. W. Coates, *Macromolecules*, 2016, **49**, 6743–6751.

10 O. Padilla-Vélez, K. S. O'Connor, A. M. LaPointe, S. N. MacMillan and G. W. Coates, *Chem. Commun.*, 2019, **55**, 7607–7610.

11 A. Hotta, E. Cochran, J. Ruokolainen, V. Khanna, G. H. Fredrickson, E. J. Kramer, Y.-W. Shin, F. Shimizu, A. E. Cherian, P. D. Hustad, J. M. Rose and G. W. Coates, *Proc. Natl. Acad. Sci. U. S. A.*, 2006, **103**, 15327–15332.

12 F. Deplace, A. K. Scholz, G. H. Fredrickson, E. J. Kramer, Y.-W. Shin, F. Shimizu, F. Zuo, L. Rong, B. S. Hsiao and G. W. Coates, *Macromolecules*, 2012, **45**, 5604–5618.

13 Z. Guan, P. M. Cotts, E. F. McCord and S. J. McLain, *Science*, 1999, **283**, 2059–2062.

14 Z. Chen and M. Brookhart, *Acc. Chem. Res.*, 2018, **51**, 1831–1839.

15 Y. Zhang, C. Wang, S. Mecking and Z. Jian, *Angew. Chem., Int. Ed.*, 2020, **59**, 14296–14302.

16 H. Mu, G. Zhou, X. Hu and Z. Jian, *Coord. Chem. Rev.*, 2021, **435**, 213802.

17 R. Murphy, M. Guo and M. Akhurst, *E4tech*, 2013, 1–16.

18 M. Khoshsefat, Y. Ma and W.-H. Sun, *Coord. Chem. Rev.*, 2021, **434**, 213788.

19 M. Delferro and T. J. Marks, *Chem. Rev.*, 2011, **111**, 2450–2485.

20 M. R. Radlauer, M. W. Day and T. Agapie, *J. Am. Chem. Soc.*, 2012, **134**, 1478–1481.

21 M. R. Radlauer, M. W. Day and T. Agapie, *Organometallics*, 2012, **31**, 2231–2243.

22 C. Boucher-Jacobs, M. Rabnawaz, J. S. Katz, R. Even and D. Guironnet, *Nat. Commun.*, 2018, **9**, 1–9.

23 D. Zhang and G. X. Jin, *Inorg. Chem. Commun.*, 2006, **9**, 1322–1325.

24 S. Sujith, D. J. Joe, S. J. Na, Y. W. Park, C. H. Choi and B. Y. Lee, *Macromolecules*, 2005, **38**, 10027–10033.

25 S. Jie, D. Zhang, T. Zhang, W. H. Sun, J. Chen, Q. Ren, D. Liu, G. Zheng and W. Chen, *J. Organomet. Chem.*, 2005, **690**, 1739–1749.

26 M. Khoshsefat, A. Dechal, S. Ahmadjo, S. M. M. Mortazavi, G. Zohuri and J. B. P. Soares, *Appl. Organomet. Chem.*, 2019, **33**, e4929.

27 S. Kong, K. Song, T. Liang, C. Y. Guo, W. H. Sun and C. Redshaw, *Dalton Trans.*, 2013, **42**, 9176–9187.

28 L. Zhu, Z. S. Fu, H. J. Pan, W. Feng, C. Chen and Z. Q. Fan, *Dalton Trans.*, 2014, **43**, 2900–2906.

29 J. M. Benito, E. De Jesús, F. De La Javier Mata, J. C. Flores, R. Gómez and P. Gómez-Sal, *Organometallics*, 2006, **25**, 3876–3887.

30 J. Wang, L. L. Ma, L. Song, S. H. Wang, H. L. Huo and C. Q. Li, *Chem. Pap.*, 2017, **71**, 895–904.

31 J. D. A. Pelletier, J. Fawcett, K. Singh and G. A. Solan, *J. Organomet. Chem.*, 2008, **693**, 2723–2731.

32 B. K. Bahuleyan, U. Lee, C. S. Ha and I. Kim, *Appl. Catal., A*, 2008, **351**, 36–44.

33 J. R. Severn, J. C. Chadwick, R. Duchateau and N. Friederichs, *Chem. Rev.*, 2005, **105**, 4073–4147.

34 A. Finiels, F. Fajula and V. Hulea, *Catal. Sci. Technol.*, 2014, **4**, 2412–2426.

35 C. Copéret, A. Comas-Vives, M. P. Conley, D. P. Estes, A. Fedorov, V. Mougel, H. Nagae, F. Núñez-Zarur and P. A. Zhizhko, *Chem. Rev.*, 2016, **116**, 323–421.

36 C. Favero, D. W. Lima, R. F. De Souza and K. Bernardo-Gusmão, *New J. Chem.*, 2017, **41**, 2333–2339.

37 P. Preishuber-Pflugl and M. Brookhart, *Macromolecules*, 2002, **35**, 6074–6076.

38 A. Dorcier, N. Merle, M. Taoufik, F. Bayard, C. Lucas, A. De Mallmann and J. M. Basset, *Organometallics*, 2009, **28**, 2173–2178.

39 M. M. Wegner, A. K. Ott and B. Rieger, *Macromolecules*, 2010, **43**, 3624–3633.

40 Y. Choi and J. B. P. Soares, *Can. J. Chem. Eng.*, 2012, **90**, 646–671.

41 S. Y. Lee and Y. S. Ko, *J. Nanosci. Nanotechnol.*, 2018, **18**, 1435–1438.

42 S. Dai and C. Chen, *Angew. Chem., Int. Ed.*, 2020, **59**, 14884–14890.

43 G. Genchi, A. Carocci, G. Lauria, M. S. Sinicropi and A. Catalano, *Int. J. Environ. Res. Public Health*, 2020, **17**, 679.

44 H. S. Schrekker, V. Kotov, P. Preishuber-Pflugl, P. White and M. Brookhart, *Macromolecules*, 2006, **39**, 6341–6354.

45 H. Tafazolian, D. B. Culver and M. P. Conley, *Organometallics*, 2017, **36**, 2385–2388.

46 H. Zhang, C. Zou, H. Zhao, Z. Cai and C. Chen, *Angew. Chem., Int. Ed.*, 2021, **60**, 17446–17451.

47 C. Tan, C. Zou and C. Chen, *J. Am. Chem. Soc.*, 2022, **144**, 2245–2254.

48 C. Boucher-Jacobs, M. Rabnawaz, J. S. Katz, R. Even and D. Guironnet, *Nat. Commun.*, 2018, **9**, 841.

49 L. C. Simon, H. Patel, J. B. P. Soares and R. F. De Souza, *Macromol. Chem. Phys.*, 2001, **202**, 3237–3247.

50 X. Fu, L. Zhang, R. Tanaka, T. Shiono and Z. Cai, *Macromolecules*, 2017, **50**, 9216–9221.

51 *Multimodal Polymers with Supported Catalysts*, ed. A. R. Albunia, F. Prades and D. Jeremic, Springer, Cham, 1st edn, 2019.

52 G. Deng, J. Luo, X. Liu, X. Zhang, Y. Wang, X. Zong and S. Xue, *Sep. Purif. Technol.*, 2022, **282**, 119993.

53 H. Tong, C. Hu, S. Yang, Y. Ma, H. Guo and L. Fan, *Polymer*, 2015, **69**, 138–147.

54 A. Jain and P. Malhotra, in *Metal-Organic Frameworks (MOFs) as Catalysts*, Springer Nature Singapore, Singapore, 2022, pp. 267–283.

55 L. C. Simon, H. Patel, J. B. P. Soares and R. F. de Souza, *Macromol. Chem. Phys.*, 2001, **202**, 3237–3247.

56 H. S. Schrekker, V. Kotov, P. Preishuber-Pflugl, P. White and M. Brookhart, *Macromolecules*, 2006, **39**, 6341–6354.

57 H. Li and T. J. Marks, *Proc. Natl. Acad. Sci. U. S. A.*, 2006, **103**, 15295–15302.

58 F. AlObaidi, Z. Ye and S. Zhu, *Macromol. Chem. Phys.*, 2003, **204**, 1653–1659.

59 F. A. Hicks, J. C. Jenkins and M. Brookhart, *Organometallics*, 2003, **22**, 3533–3545.

60 B. Wunderlich and G. Czornyj, *Macromolecules*, 1977, **10**, 906–913.

61 G. B. Galland, R. F. de Souza, R. S. Mauler and F. F. Nunes, *Macromolecules*, 1999, **32**, 1620–1625.

62 M. R. Mason, A. R. Barron, J. M. Smith and S. G. Bott, *J. Am. Chem. Soc.*, 1993, **115**, 4971–4984.

63 E. Zurek and T. Ziegler, *Prog. Polym. Sci.*, 2004, **29**, 107–148.

64 M. R. Mason, J. M. Smith, S. G. Bott and A. R. Barron, *J. Am. Chem. Soc.*, 1993, **115**, 4971–4984.

65 C. Wang, D. Zang, D. Wang, T. Xu, W. Zhong, X. Wang, Z. Fu, Q. Zhang and Z. Fan, *Inorg. Chim. Acta*, 2022, **536**, 120900.

66 A. Macchioni, *Chem. Rev.*, 2005, **105**, 2039–2074.

67 H. Li, C. L. Stern and T. J. Marks, *Macromolecules*, 2005, **38**, 9015–9027.

68 E. Y.-X. Chen and T. J. Marks, *Chem. Rev.*, 2000, **100**, 1391–1434.

69 C. Popeney and Z. Guan, *Organometallics*, 2005, **24**, 1145–1155.